2015 IEEE International Conference on Advanced Intelligent Mechatronics (AIM)
July 7-11, 2015. Busan, Korea

Atomic Force Microscopy Using Voice Coil Actuators for Vibration Isolation

Shingo Ito, Daniel Neyer, Stefan Pirker, Juergen Steininger, and Georg Schitter

Abstract— **This paper presents a vibration isolation system integrated with the internal actuators of an atomic force microscope (AFM) to vertically move the probe. For the motion, voice coil actuators (Lorentz actuators) are guided by low-stiffness flexures. Due to the low stiffness, the vibrations from the floor to the probe are decoupled at high frequencies. To reject the residual vibrations, the AFM probe tracks the AFM sample by using a displacement sensor. By mechanical and control design specifically for Lorentz actuators, the vertical motion has a control bandwidth that is 24 times higher than the first mechanical resonance to reject vibrations. As a demonstration of the vibration isolation performance, pits and tracks of a CD-ROM are successfully imaged without an external vibration isolator.**

I. INTRODUCTION

Atomic force microscopes (AFMs) are equipped with cantilevers with a sharp probe for investigating sample properties with high resolution [1]. Since these tasks are sensitive to disturbances, vibrations from the floor are a common problem for such high-precision systems [2].

Widely used countermeasures of floor vibrations are active or passive vibration isolators, where the tabletop mounting an AFM is decoupled from the floor vibrations [3]. In the case of passive vibration isolators (e.g. optical tables), the tabletop is supported by mechanical springs and dampers. These isolators show good vibration isolation at frequencies sufficiently higher than the first mechanical resonance. However, at around the resonant frequency and lower, the springs couple the tabletop and the floor, and the vibrations directly transmit to the tabletop and the AFM on it. While passive isolators are composed of springs and dampers, active vibration isolators are equipped with actuators to regulate the tabletop motion based on the vibrations measured by sensors (e.g. geophones or accelerometers) [4], [5]. Because the signal-to-noise ratio of the sensors deteriorates at low frequencies, active vibration isolators are also unable to isolate vibrations at low frequencies, similar to the passive. This limited vibration isolation performance influences the design of AFMs.

For high-quality AFM imagining on a passive or active vibration isolator, AFMs need to have mechanical resonances at sufficiently high frequencies, such that they are not excited by the vibrations reduced by the isolator (cf. [6]). Because the vibrations fluctuate the distance between the AFM probe and the sample, the mechanical loop in-between needs to be rigid and short to achieve the high resonant frequencies [1]. For such design, piezoelectric actuators, mostly used for the vertical (Z axis) motion of the probe, are ideal since they have high intrinsic stiffness between the moving part and the base. While the rigid structure can realize high-quality AFM imaging, it restricts the sample size to keep the loop short (cf. [7]). In addition, realization of a rigid structure is difficult for imagining of samples with high topography, where large Z motion is necessary. For such requirements, Lorentz actuators (i.e. voice coil actuators) guided by flexures are used as the Z actuator [8]. Since the actuators use the Lorentz force, their stiffness between the moving part and the base can be relatively freely tuned by the flexure design to determine the actuation range for a given force. Although a low stiffness is preferred for a large actuation, the mechanical loop is no longer rigid.

To isolate the floor vibrations from AFM imaging without the limitation, this paper proposes an AFM system capable of vibration isolation. In stead of conventionally used piezo actuators, the proposed system is equipped with Lorentz actuators guided by low-stiffness flexures. Due to the low stiffness, the AFM probe is isolated from the floor vibrations at high frequencies, similar to passive vibration isolators. For the rejection of the residual vibrations, the Lorentz actuators actively regulate the vertical position of the probe, such that it is always operated in its measurement range by tracking the sample. For the active control, an additional displacement sensor is installed to measure the distance between the probe and the sample. With the sensor, the vibrations along the Z axis can be distinguished from the information of interest in the AFM deflection signal for compensation [9]–[11]. Unlike active vibration isolators, the sensor measures the displacement and has high signal-to-noise ratio even at 0 Hz. By mechanical and control design specifically for the Lorentz actuators, rather than for piezos, the proposed system is even capable of imaging without an external vibration isolator.

In many cases, the Z axis motion of AFMs using flexure-guided Lorentz actuators have a control bandwidth less than the first resonant frequency with feedback control [12], [13], in the same manner as piezo-actuated systems (cf. [14]). Thus, conventional Lorentz-based Z actuation is trapped in a design trade-off between the bandwidth and the actuation stroke, as also seen in piezo-based actuators [15]. Since the first resonance of Lorentz actuators occurs at a relatively low frequency and is considered as an undesired property, high damping is preferred [12], [16]. In the case of the proposed system design, however, the Z actuators attain a control

*This work has been supported in part by the Austrian Research Promotion Agency (FFG) under project number 836489.

S. Ito, D. Neyer, S. Pirker, J. Steininger, and G. Schitter are with Automation and Control Institute (ACIN), Vienna University of Technology, 1040 Vienna, Austria ito@acin.tuwien.ac.at.

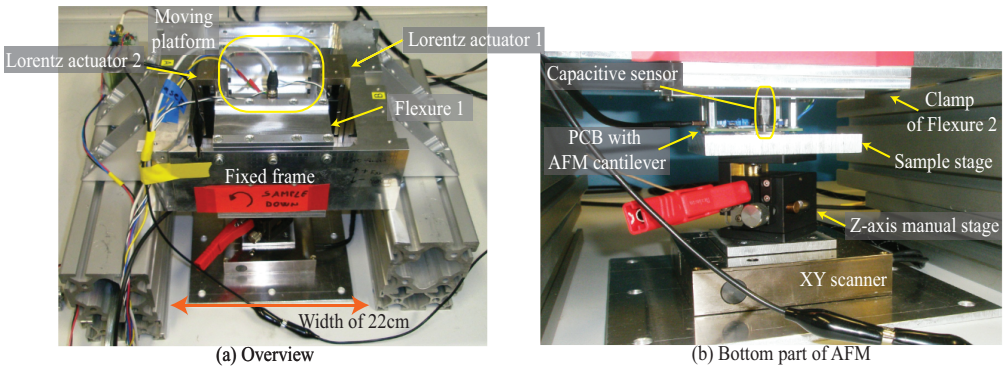

Fig. 1. Photograph of AFM vibration isolation system showing overview (a) and bottom part (b).

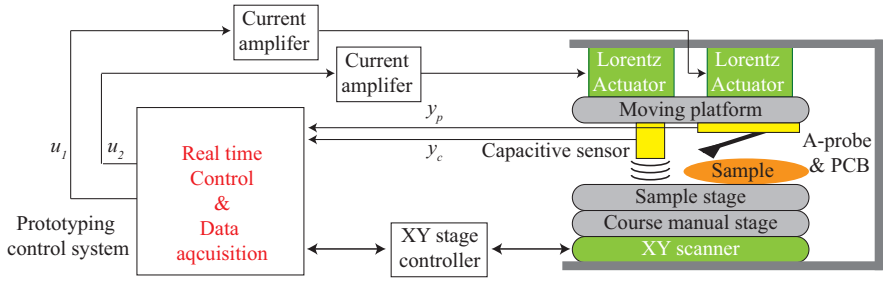

Fig. 2. Block diagram of AFM vibration isolation system with electronics, where u_1 and u_2 are the references to the current amplifiers. Output voltage y_c is form the capacitive sensor, while y_p is from the A-probe PCB.

bandwidth much higher than the first resonant frequency. Such actuators combine passive and active vibration isolation [17], and they are able to position with nanometer resolution without an external vibration isolator [18]. Furthermore, the Z actuation of the proposed system is no longer trapped in the bandwidth-range dilemma. In addition, the AFM vibration isolation system uses the high gain of the first resonance to reject vibrations, treating it as beneficial properties.

II. System Description

Fig. 1 shows the proposed AFM system on a laboratory table without a vibration isolator. The moving platform to accommodate an AFM probe is mechanically guided along the vertical axis (Z axis) by two parallel flexures and is actuated by two Lorentz actuators (AVA 2-20, Akribis Systems, Singapore). Their relatively heavy magnets are stiffly connected to the fixed frame, while the coils are connected to the moving platform to achieve the light weight of the platform (i.e. moving-coil configuration). Since the Lorentz force is proportional to the coil current, current amplifiers are designed to drive the actuators and implemented by analog circuits to provide a high bandwidth of 21 kHz (-3dB).

To measure and control vibrations, a capacitive displacement sensor (6810(6504-01), MicroSense, Lowell, USA) is mounted on the moving platform. If the displacement sensor is compatible with the AFM sample, it can measure the distance to the sample directly. In this case, the sample can be as large as 220 mm, due to the large space under the moving platform (Fig. 1(a)). To focus on the demonstration of the vibration immunity in this paper, however, the capacitive sensor measures the distance between the moving platform and the sample stage, which is placed on top of a manual stage for the coarse Z axis adjustment (Fig. 1(b)). The sample stage and the manual stage are mounted on an piezoelectric XY scanner (NPXY100-100, nPoint, Middleton, USA) for AFM imaging. The scanner is driven by a controller (LC.402, nPoint, Middleton, USA), where the internal integral controllers with notch filters are tuned for each motion axis.

For the experiments in this paper, an Akiyama probe (A-probe) (A-PROBE-10, Nanosensors, Neuchatel, Switzerland) is used as the AFM probe for simplicity of implementation, because it requires no optical components [19]. An A-probe is a self-sensing and self-actuating probe using a quartz tuning fork, and oscillates at its resonant frequency of approximately 45 kHz, which varies dependent on the distance between the tip and the sample. Due to its tip radius smaller than 15 nm, the probe has a high lateral resolution, unlike the capacitive sensor. To operate the probe for the tip-sample-distance measurement, a PCB is implemented and attached to the backside of the moving platform, holding the A-probe. For the calibration of the A-probe, the capacitive sensor is used, and the platform is vertically moved by the Lorentz actuators under feedback control (Section IV). The probe has a measurement range of approximately 1.5 μm and a sensitivity of $K_p = 1.17$ V/μm.

As shown in Fig. 2, the current amplifiers, the XY stage controller, the capacitive sensor, and the A-probe PCB are all connected to a rapid prototyping control system (DS1005,

dSPACE GmbH, Paderborn, Germany), where controllers are implemented at a sampling frequency of $f_s = 20\,\text{kHz}$. The signals u_1 and u_2 are the input signals to the current amplifiers. The voltage y_c is the output of the capacitive sensor. The A-probe PCB outputs y_p, which is proportional to the tip-sample distance.

III. System Analysis

A. Over-actuation

While the bandwidth of a Lorentz actuator can be higher than the first resonant frequency with feedback control [17], it is limited by higher resonant frequencies due to internal modes [20]. To achieve a high control bandwidth for the proposed system, although one actuator is sufficient for the Z axis motion, two Lorentz actuators are installed to prevent the Z actuation from exciting rotational modes resulting from the platform inertia and flexures.

The concept to avoid the excitation of the undesired modes is illustrated in Fig. 3, where a coordinate frame is attached to the center of gravity (COG) of the moving platform. The actuator coil 1 and 2 provide the actuation force F_1 and F_2, respectively. These forces generate a torque τ_x around the X axis as follows

$$\tau_x = L_2 F_2 - L_1 F_1, \tag{1}$$

where L_1 and L_2 are the distances from the coil 1 and 2 to the COG along the Y axis, respectively. Since F_1 and F_2 are proportional to the respective amplifier reference u_1 and u_2, τ_x is zero under the following reference ratio r_u

$$r_u = u_1/u_2 = F_1/F_2 = L_2/L_1. \tag{2}$$

By keeping the above ratio, the moving platform can vertically move without exciting the rotational modes around the X axis. The advantage of this method is that (2) can be satisfied at the control design phase of the mechatronic system design. Thus, the rotational modes can still be avoided without redesigning the mechanical structure, even if the components on the moving platform are modified (e.g. replacement of the capacitive sensor or the PCB with the A-probe).

In the implementation, r_u is set at one ($u_1 = u_2 = u$), because the A-probe PCB is relatively light and the moving platform is symmetrically designed about the ZX plane. For the validation of the reference tuning, Bode plots are measured from u to the capacitive sensor output y_c on an optical table for better signal-to-noise ratio. Fig. 4 compares when only one Lorentz actuator is active and when both are active with $r_u = 1$. Since the two actuators prevents the excitation of the resonances between 300 Hz and 500 Hz, the corresponding magnitude shows a smooth -40 dB/dec line in the frequency domain.

The redundant actuators for the high control bandwidth is fundamentally different from an approach used for piezo-actuated systems, where unwanted rotational resonances are shifted to high frequencies by increasing the corresponding spring constant of the flexures [15]. Dependent on the requirements on the flexure size, such an approach may also

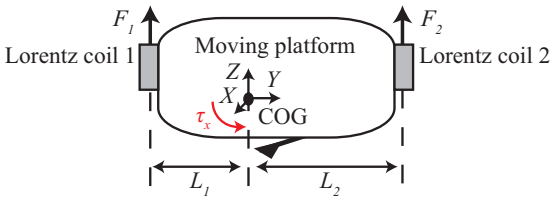

Fig. 3. Conceptual cross-sectional view of moving platform with coordinate frame at its center of gravity. The Lorentz coil 1 and 2 exert force F_1 and F_2, respectively, creating a torque τ_x around the X axis.

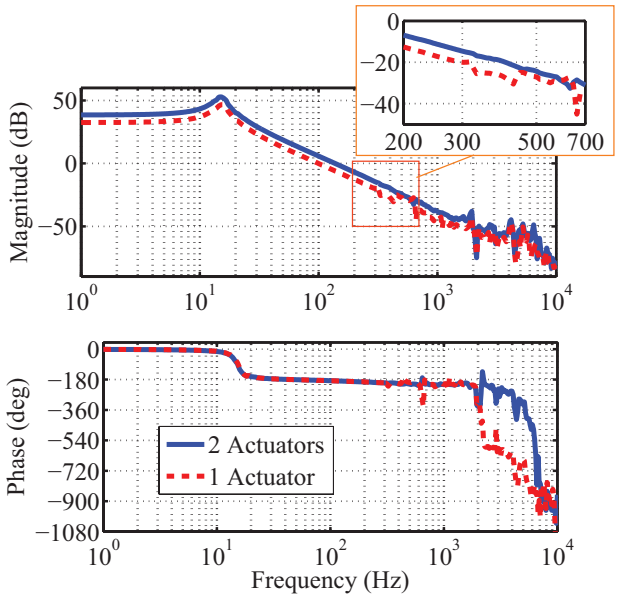

Fig. 4. Measured Bode plot from amplifier reference u to capacitive sensor output y_c, when both Lorentz actuators are turned on with $r_u = 1$ (a), and when only one of them is turned on (b).

increase the spring constant of the actuation axis, reducing the motion range. However, at least in the case of Lorentz actuators, over-actuation by the redundant actuators break through the design trade-off. Fig. 4 clearly shows that the existence of mechanical resonances itself is not an obstacle for a high bandwidth, as long as they are not excited. In other words, the undesired mechanical modes can be rendered uncontrollable by the over-actuation [21]. If they are stable (i.e. stabilizable), they do not have to be considered in the control design.

B. Modeling

For control design, the AFM system is modeled for the vertical actuation as shown in Fig. 5, where k and c are the spring constant and the damping coefficient of the flexures. The moving platform has a mass of $m = 0.86\,\text{kg}$, and its vertical position is represented by z_m. While the symbols z_f and z_s are positions of the fixed frame and the sample stage, z_h is the sample height including features to be imaged. The actuation force of the Lorentz actuators are summed up as F with the reference ratio r_u chosen not to excite the rotational modes. From the lumped mass model, an equation of motion

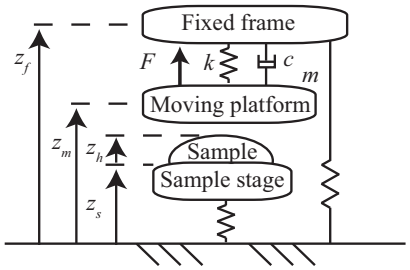

Fig. 5. Lumped mass model of AFM vibration isolation system.

can be derived as follows

$$m\ddot{z}_m + c(\dot{z}_m - \dot{z}_f) + k(z_m - z_f) = F. \tag{3}$$

After the Laplace transformation, the platform position is given as follows

$$Z_m(s) = P_a(s)(F(s) + P_d(s)Z_f(s)), \tag{4}$$

using

$$P_a(s) = Z_m(s)/F(s) = (ms^2 + cs + k)^{-1}, \tag{5}$$

$$P_d(s) = cs + k, \tag{6}$$

where $Z_m(s)$, $Z_f(s)$ and $F(s)$ are the Laplace transformations of z_m, z_f and F. While the transfer function $P_d(s)$ represents the mechanical coupling between the moving platform and the fixed frame, $P_a(s)$ represents the platform position z_m resulting from the applied force on it.

As the probe measures the distance between the platform and the sample surface, its output voltage is given as follows

$$Y_p(s) = K_p(Z_m(s) - Z_s(s) - Z_h(s)), \tag{7}$$

where $Z_s(s)$, $Z_h(s)$ and $Y_p(s)$ are the Laplace transformation of z_s, z_h, and y_p, respectively. Similarly, the output voltage of the capacitive sensor $Y_c(s)$, the Laplace transformation of y_c, is given as

$$Y_c(s) = K_c(Z_m(s) - Z_s(s)), \tag{8}$$

where K_c is the capacitive sensor's sensitivity of 0.2 V/μm. Since both the current amplifiers receive the same reference signal u as discussed, the transfer function from u to F is

$$P_e(s) = \frac{F(s)}{U(s)} = 2K_{ca}K_a\frac{1 - \frac{\tau}{2}s}{1 + \frac{\tau}{2}s}, \tag{9}$$

where $U(s)$ is the Laplace transformation of u, and K_a is the motor constant of the Lorentz actuators (approximately 7.2 N/A). The parameter τ is a delay represented by the first-order Pade approximation to capture the phase lag of the current amplifiers with a gain of $K_{ca} = 200$ mA/V. From (4) and (7) - (9), the AFM vibration isolation system can be modeled as shown in Fig. 6. For the control design to tack the sample, the transfer function from u to y_c is given as follows

$$P(s) = Y_c(s)/U(s) = K_cP_a(s)P_e(s). \tag{10}$$

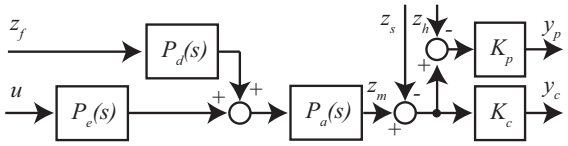

Fig. 6. Block diagram of modeled system, where u is the current amplifier reference with sample height z_h. y_p and y_c are the outputs of the probe and the capacitive sensor. Vibrations z_f and z_s are regarded as disturbances.

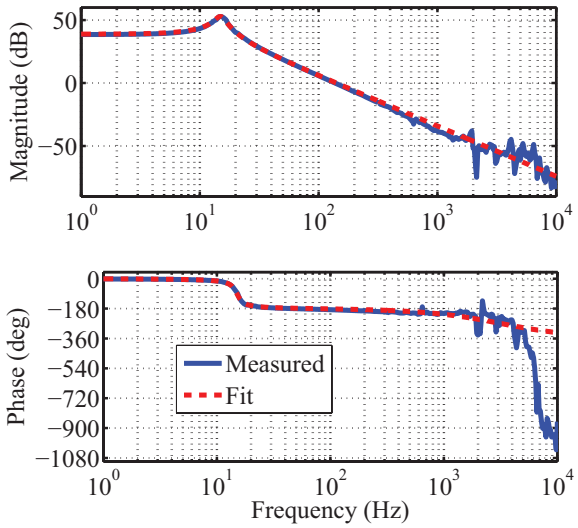

Fig. 7. Measured Bode plot from u to y_c used for estimation of unknown parameters and simulated frequency response of resulting model (10).

C. Parameter estimation and modeling error

Unknown parameters are estimated by fitting a simulated Bode plot of (10) to the measured Bode plot with the two Lorentz actuators in Fig. 4. The fitting results with $k = 7.65$ kN/m, $c = 16.23$ N/(m/s), and $\tau = 100$ μs are shown in Fig. 7. While the first resonance at 15 Hz due to the suspension mode is well-modeled, the high-frequency resonances are not captured to keep the order of the model low to simplify the control design.

The fitting error can be quantized as the multiplicative uncertainty Δ_m [22] given as

$$\Delta_m(j\omega) = |P_m(j\omega)/P(j\omega) - 1|, \tag{11}$$

where $P_m(j\omega)$ represents the measured frequency response (blue-solid line of Fig. 7). For control design, the upper bound of $\Delta_m(j\omega)$ is approximated by a low-order transfer function $W_T(s)$, which is tuned to cover $\Delta_m(j\omega)$, as shown in Fig. 8 [22] and is given by the following equation

$$W_T(s) = 0.65\frac{s^2/(2\pi\cdot 800)^2 + 1.4s/(2\pi\cdot 800) + 1}{s^2/(2\pi\cdot 9000)^2 + 1.4s/(2\pi\cdot 9000) + 1}. \tag{12}$$

IV. Control Design

Equation (7) implies that the sample height z_h can be measured by the probe without the vibrations of z_s and z_f when the moving platform tracks the sample stage (i.e. $z_m = z_s$). This can be realized by feedback control using the capacitive

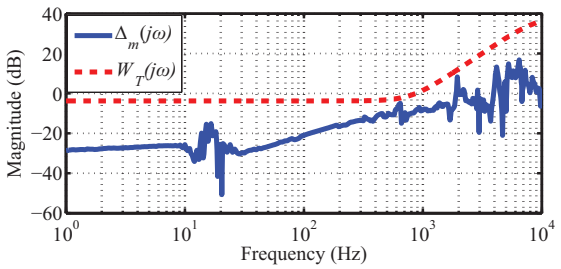

Fig. 8. Multiplicative uncertainty $\Delta_m(j\omega)$ representing fitting error and its upper bound $W_T(s)$.

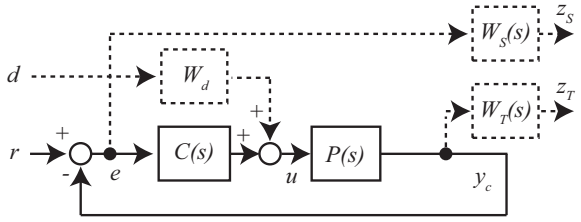

Fig. 9. Control block diagram to regulate Lorentz actuators, where r and e are position reference and error. Additional signal d and weights W_d, $W_S(s)$ and $W_T(s)$ are used for control design.

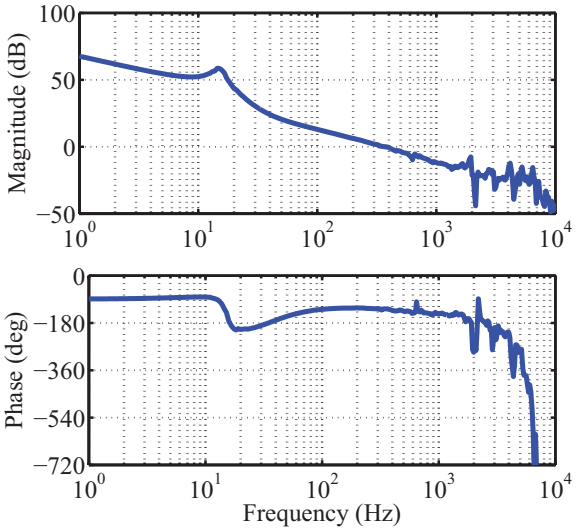

Fig. 10. Simulated open-loop transfer function $C(s)P_m(s)$.

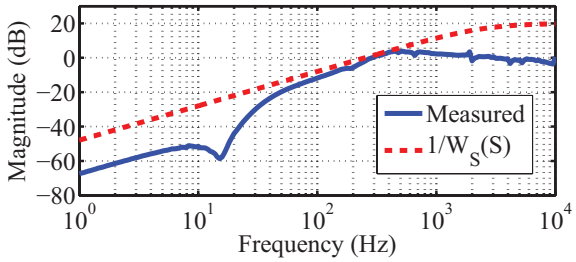

Fig. 11. Measured sensitivity function $S(s)$ for validation of control design and implementation with inverse of its weight $1/W_S(s)$.

sensor signal y_c. The advantage of the configuration is that the vibration isolation performance does not depend on the A-probe, the sensitivity of which would be different for each product.

For the feedback control design, H_∞ control synthesis [23] is used to guarantee stability with the fitting error. The design is based on Fig. 9, where r and e are the position reference and the error. While $W_T(s)$ is used as the weight on the complementary sensitivity function $T(s)$ to consider the model uncertainty, $W_S(s)$ has low-pass characteristics as the weight on the sensitivity function $S(s)$ for good vibration rejection. An additional signal d is added, and its constant weight W_d is tuned to prevent the controller zeros from canceling the poles of $P(s)$. By doing so, the first resonance contributes to the disturbance rejection [17]. The controller $C(s)$ is obtained by minimizing the H_∞ norm of the transfer function from r and e to the weighted signals z_S and z_T. For a high control bandwidth, $W_S(s)$ is tuned, such that its cross-over frequency is maximized under the condition that the minimized norm is less than one for guaranteeing stability and robustness [23].

The simulated open-loop transfer function $P_m(s)C(s)$ in Fig. 10 shows its unit-gain cross-over frequency at 370 Hz. This is 24 times higher than the first mechanical resonant frequency at 15 Hz of the suspension mode. Since the controller does not cancel the plant poles, the first resonance increases the open-loop gain at that frequency. As a result, it contributes to the vibration rejection, showing a deep notch in the measured $S(s)$ of Fig. 11. For this reason, a low damping coefficient c may even be desirable in the mechanical design, which also benefits the reduction of the mechanical coupling (6) to decrease the transmission of vibration z_f. Note that these control properties cannot be attained by PI or PII controls with piezoelectric actuators, which are often used for the Z actuation in AFMs [24], because they cannot provide phase lead for closed-loop stability beyond the first resonant frequency.

V. Experiments

For experimental validation, a CD-ROM is used as an AFM sample, because it is easily obtainable and has well-defined features. As the sample preparation, the reflective coating is stripped from the transparent polycarbonate layer. The exposed polycarbonate surface has hollow pits, representing the data on the disk. The pit width is 0.50 μm, and the data tracks have a distance of 1.6 μm [25].

For the scanning of the polycarbonate surface, a ramp signal and a triangular signal of 10 Hz are generated as the inputs to the XY stage controller by the prototyping control system. To generate an AFM image, it also records the triangular signal and the probe signal y_p. As the post processing after recording, the mean of the data set of y_p is removed, and the scale is corrected by the probe sensitivity. Fig. 12 shows the generated AFM images. When the Lorentz actuators for vibration isolation and surface tracking are turned off, the image does not show any meaningful features, due to the floor vibrations (Fig. 12(a)). In contrast,

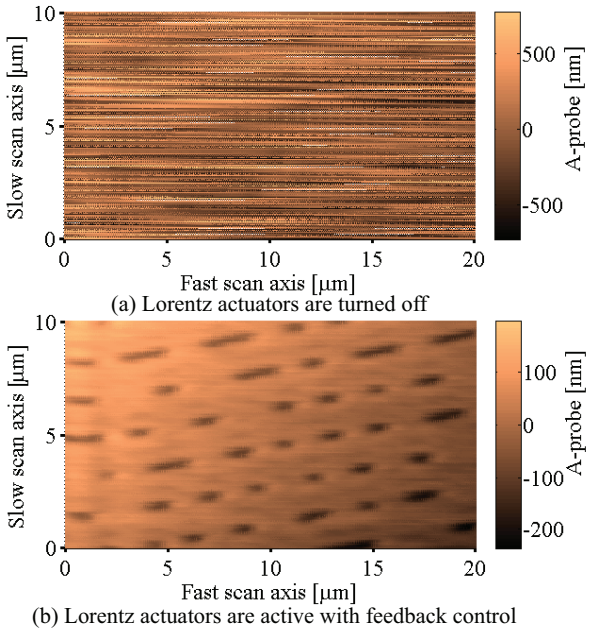

(a) Lorentz actuators are turned off

(b) Lorentz actuators are active with feedback control

Fig. 12. AFM images of CD-ROM measured when Lorentz actuators are turned off (a) and when they are turned on with feedback control (b).

by enabling the Lorentz actuators and the feedback control, the pits and tracks are successfully imaged without using an external vibration isolator (Fig. 12(b)).

Additionally to evaluate the vibration isolation, the capacitive sensor output y_c is recorded as the sample tracking error due to vibrations. When the Lorentz actuators are turned off, the standard deviation of y_c is $\sigma = 385\,\text{nm}$. By using the actuators with the feedback control, this error is decreased by 98 % to $\sigma = 7.4\,\text{nm}$ for AFM imaging. These results successfully demonstrate the integration of vibration isolation with vertical tracking of the sample surface by means of low-stiffness flexure-guided Lorentz actuators.

VI. Conclusion

A vibration isolation system is integrated with Lorentz actuators for the Z axis motion in an AFM system. While two Lorentz actuators are installed to prevent the excitation of the undesired mechanical resonances for high control bandwidth, an additional capacitive sensor is for measuring the vibrations between the AFM probe and the sample. By carefully designing the feedback controller, the Z axis attains a control bandwidth (open-loop cross-over frequency) of 370 Hz, which is 24 times higher than the first resonant frequency at 15 Hz. As a result, the AFM system is operational without an external vibration isolator, as is successfully demonstrated by imaging the pits and tracks of a CD-ROM.

References

[1] P. Eaton and P. West, *Atomic Force Microscopy*. Oxford University Press, 2010.

[2] H. Amick, M. Gendreau, T. Busch, and C. Gordon, "Evolving criteria for research facilities I: vibration," in *Proc. SPIE 5933*, vol. 5933, 2005, p. 593303.

[3] R. Munnig Schmidt, G. Schitter, and J. van Eijk, *The Design of High Performance Mechatronics*. Delft University Press, 2014.

[4] J. Hong and K. Park, "Design and control of six degree-of-freedom active vibration isolation table," *Review of Scientific Instruments*, vol. 81, no. 3, pp. –, 2010.

[5] G. Balik, B. Caron, J. Allibe, A. Badel, J.-P. Baud, L. Brunetti, G. Deleglise, A. Jeremie, R. Le Breton, and S. Vilalte, "Sub-nanometer active seismic isolator control," *Journal of Intelligent Material Systems and Structures*, vol. 24, no. 15, pp. 1785–1795, 2013.

[6] C. Kim, J. Jung, W. Youm, and K. Park, "Design of mechanical components for vibration reduction in an atomic force microscope," *Review of Scientific Instruments*, vol. 82, no. 3, pp. –, 2011.

[7] Q. Wang, Y. Hou, J. Wang, and Q. Lu, "A high-stability scanning tunneling microscope achieved by an isolated tiny scanner with low voltage imaging capability," *Review of Scientific Instruments*, vol. 84, no. 11, pp. –, 2013.

[8] H. Barnard, C. Randall, D. Bridges, and P. K. Hansma, "The long range voice coil atomic force microscope," *Review of Scientific Instruments*, vol. 83, no. 2, pp. –, 2012.

[9] G. Schitter and A. Stemmer, "Eliminating mechanical perturbations in scanning probe microscopy," *Nanotechnology*, vol. 13, no. 5, pp. 663–665, 2002.

[10] A. W. Sparks and S. R. Manalis, "Atomic force microscopy with inherent disturbance suppression for nanostructure imaging," *Nanotechnology*, vol. 17, no. 6, pp. 1574–1579, 2006.

[11] C. Kim, J. Jung, and K. Park, "Note: Vibration reduction control of an atomic force microscope using an additional cantilever," *Review of Scientific Instruments*, vol. 82, no. 11, pp. –, 2011.

[12] W. Youm, J. Jung, S. Lee, and K. Park, "Control of voice coil motor nanoscanners for an atomic force microscopy system using a loop shaping technique," *Review of Scientific Instruments*, vol. 79, no. 1, pp. –, 2008.

[13] C. Werner, P. Rosielle, and M. Steinbuch, "Design of a long stroke translation stage for AFM," *International Journal of Machine Tools and Manufacture*, vol. 50, no. 2, pp. 183 – 190, 2010.

[14] A. J. Fleming, "Nanopositioning system with force feedback for high-performance tracking and vibration control," *IEEE/ASME Transactions on Mechatronics*, vol. 15, no. 3, pp. 433–447, June 2010.

[15] Y. K. Yong, S. O. R. Moheimani, B. J. Kenton, and K. K. Leang, "Invited review article: High-speed flexure-guided nanopositioning: Mechanical design and control issues," *Review of Scientific Instruments*, vol. 83, no. 12, pp. –, 2012.

[16] T. Mariani, C. Frediani, and C. Ascoli, "A three-dimensional scanner for probe microscopy on the millimetre scale," *Applied Physics A*, vol. 66, pp. S861–S866, March 1998.

[17] S. Ito and G. Schitter, "Comparison and classification of high-precision actuators based on stiffness influencing vibration isolation (Submitted)," *IEEE/ASME Transactions on Mechatronics*, 2014.

[18] S. Ito, J. Steininger, and G. Schitter, "Low-stiffness dual stage actuator for long range positioning with nanometer resolution (Accepted)," *Mechatronics*, 2015.

[19] T. Akiyama, U. Staufer, N. F. de Rooij, P. Frederix, and A. Engel, "Symmetrically arranged quartz tuning fork with soft cantilever for intermittent contact mode atomic force microscopy," *Review of Scientific Instruments*, vol. 74, no. 1, pp. 112–117, 2003.

[20] D.-J. Lee, M.-G. Song, C. Kim, N.-C. Park, Y.-P. Park, N. Onagi, and G. Akanuma, "Improvement of dynamic characteristics for symmetric-type slim optical pickup actuator by changing coil shape," *IEEE Transactions on Magnetics*, vol. 43, no. 2, pp. 808–810, Feb 2007.

[21] M. J. C. Ronde, M. G. E. Schneiders, E. J. G. J. Kikken, M. J. G. van de Molengraft, and M. Steinbuch, "Model-based spatial feedforward for over-actuated motion systems," *Mechatronics*, vol. 24, no. 4, pp. 307 – 317, 2014.

[22] T. Yamaguchi, M. Hirata, and C. Pang, *High-Speed Precision Motion Control*. Taylor & Francis, 2011.

[23] S. Skogestad and I. Postlethwaite, *Multivariable Feedback Control*. John Wiley, 2005.

[24] D. Y. Abramovitch, S. B. Andersson, L. Y. Pao, and G. Schitter, "A tutorial on the mechanisms, dynamics, and control of atomic force microscopes," in *American Control Conference*, July 2007, pp. 3488–3502.

[25] K. Clements, *Understanding and Servicing CD Players*. Newnes, 1994.